ANALYSIS OF THE RESPONSE OF A DEFORMABLE STRUCTURE TO UNDERWATER EXPLOSION BUBBLE LOADING USING A FULLY COUPLED FLUID-STRUCTURE INTERACTION PROCEDURE

Kenneth M. Kalumuck, Georges L. Chahine, Ramani Duraiswami
DYNAFLOW, INC.
7210 Pindell School Road
Fulton, MD 20759
(301) 604-3688

The dynamics of bubbles and their interaction with nearby bodies, in the absence of structural deformations, have been studied effectively using boundary element method (BEM) based computer programs. However, structural motion and deformation effects can be important for accurately determining the bubble dynamics and the resulting structural loads. Reliable prediction of bubble loading and the resulting structural response requires both accurate simulation of the bubble dynamics prior and subsequent to reentrant jet touchdown and fully coupled fluid-structure interaction modeling. We have developed BEM based codes to study nonlinear free surface flows in three-dimensional (**3DynaFS**) and axisymmetric (**2DynaFS**) geometries. Progress in coupling these fluid codes to existing finite element structural codes (NIKE3D and NIKE2D) are reported. The results indicate the local structural response influences the bubble dynamics resulting in modification of the bubble shape, bubble period, reentrant jet formation, and pressures generated on the structure.

INTRODUCTION

The Boundary Element Method (BEM) has proven to be very efficient in solving bubble dynamics problems. A number of researchers have employed the BEM to model axisymmetric problems of bubble dynamics near infinite walls (e.g., [1-4]). Chahine et. al. [5-7] extended the method to three-dimensional bubble dynamics problems. This effort resulted in the development of the BEM codes **3DynaFS** (three-dimensional) and **2DynaFS** (axisymmetric) for the study of problems with nonlinear free surface deformations.

In this paper, we present results of efforts to create an integrated fluid-structure analysis capability. The approach we have taken to achieve this is to utilize two different types of codes: BEM codes for the fluid/bubble dynamics and finite element codes for the structural dynamics. This enables one to take advantage of the strengths and efficiencies inherent in each code: accurate free surface hydrodynamics and sophisticated structural and material models.

The structural analysis is performed using the NIKE suite of finite element programs developed by Lawrence Livermore National Laboratories (LLNL) [8,9] which can handle both geometric (large strain) and material nonlinearities. In the work reported here, a linear elastic material model was employed. Four-noded axisymmetric elements were selected with the axisymmetric code, while for three-dimensional modeling, both quadrilateral and triangular shell elements were employed. Implicit structural codes were selected to allow stability to be maintained while allowing the time step to be determined by the fluid code, thus enabling adaptive time stepping during the bubble oscillations.

MODEL FORMULATION

Two coupled programs have been developed: one that couples **2DynaFS** and NIKE2D for axisymmetric problems, and another that couples **3DynaFS** and NIKE3D for three-dimensional problems.

Shortly after the bubble generation and following propagation of a shock wave away from the explosion center, large subsonic bubble wall velocities are observed, and one can neglect viscosity and compressibility effects on the bubble dynamics. These assumptions result in a potential flow (velocity potential, Φ) satisfying the Laplace equation,

$$\nabla^2\Phi = 0. \tag{1}$$

Coupled Numerical Procedure

Both coupled codes employ a complete coupling of the fluid and the structure at the wetted surfaces of the structure. Calculations are performed at each time step for both the fluid and the structure. Pressures calculated in the fluid are passed to the structure as loads. Velocities and displacements calculated by the structure code are passed to the fluid code. The algorithms are structured such that the fluid code is the "main" routine while the structural code functions as a set of subroutines driven by the "main" fluid routine.

A fully coupled analysis is carried out using the following procedure:

- Read input data, initialize fluid and solid routines, and begin time stepping.
- (*) Solve boundary element equations in the fluid.
- Compute pressure at each node by use of the unsteady Bernoulli equation.
- Pass pressures to structural code as loads at each structure node.
- Solve the structural equations with this new load, knowing the state of the structure at the previous time step, to obtain the new displacement, velocity and acceleration of each node of the structure.
- Pass new velocities and displacements to the fluid code as new boundary conditions.
- Set the velocity normal to the structure at each fluid node along the wetted surface equal to the normal component of the gradient of the potential, $\partial\Phi/\partial n$, at that point.
- Update the position of the wetted surface.
- Increment time and return to (*).

RESULTS AND DISCUSSION

The results of a series of calculations that highlight the effects of structural motion on bubble dynamics are presented here. In these calculations characteristic length, pressure and time scales are given by $R_{\max}$, the maximum radius the bubble would achieve in an infinite medium; P_o, the ambient pressure at the location of the initial center of the bubble; and T, the Rayleigh bubble time - the natural period of a bubble in an infinite medium and in the absence of gravity given by

$$T = R_{\max}\sqrt{\frac{\rho}{P_o}}. \tag{7}$$

Pressure Loading and Post Touchdown Calculations

Two critical features of any bubble loading simulation method are the calculation of the pressure loading on the body and the ability to calculate bubble behavior, including pressures generated past reentrant jet touchdown. In order to validate the BEM scheme we have developed for such bubble dynamics simulations, we utilized **2DynaFS** to simulate experiments conducted by NSWC at Seneca Lake [18]. Details of the comparisons and the numerical implementation are provided in [13]. Example results for Shot No. 1 of these tests are presented here. The experiments were conducted with a simple axisymmetric flat plate target geometry: a 70-inch diameter, 1-inch thick, circular steel plate. Bolted into the center of the plate was a 1-foot diameter, 6-inches thick aluminum target plug instrumented with pressure gages. The arrangement enabled the target to be essentially rigid (i.e., non-compliant). A charge of 10.3 g of CH-6 (cyclohexane) was detonated at a depth of approximately 166.5 ft. The target plate was located at a standoff distance of 0.465 ft. computed to correspond to 0.75 R_{max}.

Figure 1 presents the calculated pressure contours and velocity vectors at three selected times just prior to, at, and subsequent to reentrant jet impact. Shown are the impact of the reentrant jet and post touchdown behavior of the remaining toroidal bubble. At impact (t=15.5 ms.), the high pressures are observed on the wall, caused by breakthrough and subsequent impact on the wall. As the jet spreads out, the loaded area increases and the pressure magnitudes begin to decrease. When the bubble nears its minimum volume (t=16.8 ms.), a much larger area is affected by this lower intensity pressure pulse.

The potential, Φ, must satisfy initial and boundary conditions at the bubble wall, on the boundaries of any nearby bodies, and at infinity. At all solid surfaces we equate the normal velocities of the fluid and the surface:

$$\nabla\Phi \cdot \mathbf{n} = \mathbf{V}_s \cdot \mathbf{n}, \tag{2}$$

where $\mathbf{n}$ is the local unit vector normal to the surface and $\mathbf{V}_s$ is the local velocity vector of the surface.

The pressure in the liquid at the bubble surface, P_L, is obtained at any time from the following pressure balance equation:

$$P_L = P_v + P_{g_0}\left(\frac{\mathcal{V}_0}{\mathcal{V}}\right)^k - \mathcal{C}\sigma, \tag{3}$$

where P_{g_0} and $\mathcal{V}_0$ are the initial known bubble gas pressure and volume respectively, k a polytropic constant $(1 < k < c_p/c_v)$, σ is the surface tension, $\mathcal{C}$ is the local curvature of the bubble, and $\mathcal{V}$ is the instantaneous value of the bubble volume.

Boundary Element Formulation

The Boundary Element Method was chosen because of its computational efficiency. By considering only the boundaries of the fluid domain it reduces the dimension of the problem by one. This method is based on Green's equation which provides Φ anywhere in the domain of the fluid (field points P) if the velocity potential, Φ, and its normal derivatives are known on the fluid boundaries (points M),

$$\int\int_s \left[-\frac{\partial\Phi}{\partial n}\frac{1}{|\,\mathbf{MP}\,|} + \Phi\frac{\partial}{\partial n}\left(\frac{1}{|\,\mathbf{MP}\,|}\right)\right] ds = a\pi\Phi(P), \tag{4}$$

where $a\pi = \Omega$ is the solid angle under which P sees the fluid. If the field point is selected to be on the boundary of the domain of integration, then a closed set of equations can be obtained and used at each time step to solve for values of $\partial\Phi/\partial n$ (or Φ) assuming that all values of Φ (or $\partial\Phi/\partial n$) are known at the preceding step.

To solve Equation (4) numerically, it is necessary to discretize the geometry into panels, perform the integration over each panel, and sum up the contributions of all panels. Equation (4) then becomes a set of N equations (N is the number of discretization nodes) of index i of the type:

$$\sum_{j=1}^{N}\left(A_{ij}\frac{\partial\Phi_j}{\partial n}\right) = \sum_{j=1}^{N}(B_{ij}\Phi_j) - a\pi\Phi_i, \tag{5}$$

where A_{ij} and B_{ij} are elements of matrices which are the discrete equivalent of the integrals given in Equation (4).

To obtain the total fluid velocity at any point on the boundary, the tangential velocity, $\mathbf{V_t}$, must be computed in addition to the normal velocity, $\mathbf{V_n} = \partial\Phi/\partial n\ \mathbf{n}$. This is done using a local surface fit to the velocity potential.

The basic procedure can then be summarized as follows. With the problem initialized and the velocity potential known over the free surfaces (such as the bubble interface), an updated value of $\partial\Phi/\partial n$ can be obtained by performing the integrations in (4) and solving the corresponding matrix equation (5). $D\Phi/Dt$, the material derivative of the potential is then computed using Bernoulli's equation:

$$\frac{D\Phi}{Dt} = \frac{\partial\Phi}{\partial t} + \nabla\Phi\cdot\nabla\Phi = \frac{\partial\Phi}{\partial t} + |\,\mathbf{V}\,|^2\,. \tag{6}$$

Using an appropriate time step the values of Φ on the boundaries can be updated using Φ at the previous time step and $D\Phi/Dt$. New coordinate positions of the nodes are then obtained using the displacement:

$$d\mathbf{M} = \left(\frac{\partial\Phi}{\partial n}\mathbf{n} + V_t.\mathbf{e}_t\right)dt,$$

where $\mathbf{n}$ and $\mathbf{e}_t$ are the unit normal and tangential vectors. This time stepping procedure is repeated throughout the bubble growth and collapse, resulting in a shape history of the bubble. These BEM codes have been validated against Rayleigh-Plesset solutions and available 2-D and 3-D experimental results [5,6,11].

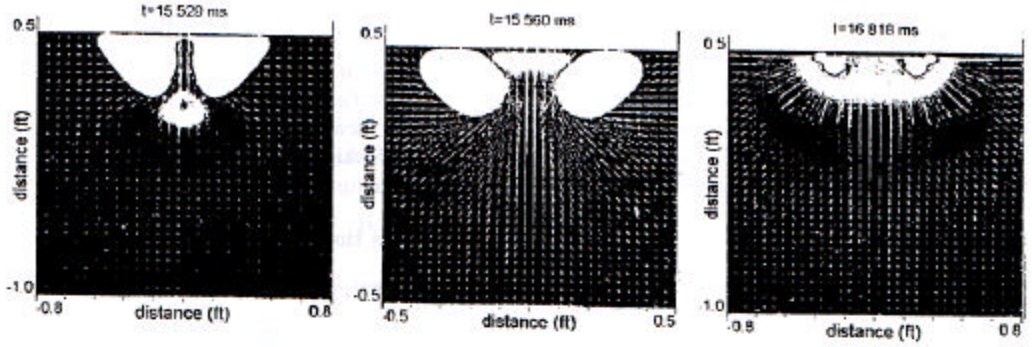

Figure 1: Pressure and Velocity Fields Calculated by **2DynaFS** Prior to and Following Reenetrant Jet Touchdown.

These calculated results are compared to the measured experimental data in Figure 2, which compares the pressures at the center of the target plate near the time of bubble collapse. For clarity, the early-time shock wave pressures and long duration underpressure phase while the bubble is expanding and contracting are not shown here. The comparison of the measured and calculated pressures show excellent agreement.

The timing of the jet touchdown (impact on the plate) is well reproduced by the **2DynaFS** calculation, which matches the experimental value of 15.5 ms. The overall pressure history also reproduces the physical phenomena measured in the experiment. The initial rise in the pressure record is due to the impact of the jet on the wall. The calculation reproduces the early twin peak behavior and the overall magnitude of the impact event. The **2DynaFS** results also capture the pressures associated with the contraction of the bubble to its minimum volume, which appear as the secondary peak in the measured data at approximately 16.9 ms.

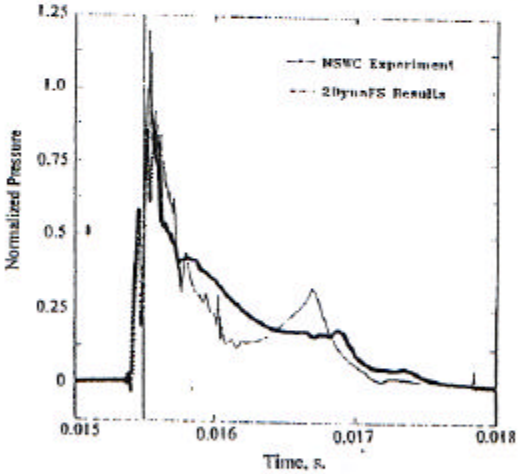

Figure 2: Comparison of Pressure History at Center of Target Plate Calculated by **2DynaFS** with Measured Values for Seneca Lake Shot 1.

Deforming Axisymmetric Flat Plate Structure

As an initial example, calculations were carried out by coupling **2DynaFS** to a relatively simple axisymmetric finite element code, DYNAMIC, developed by the NSWC Carderock Division [12]. An explosion bubble generated beneath a large circular plate with a rigid outer section and a flexible central section was considered. The bubble is generated at a depth of 167 ft. by a charge weight of 10.3 grams of CH-6 at a standoff of 0.75 R_{max}. The large plate of thickness $R_{max}/32$ consists of a central (inner) flexible portion of radius R_f =2.5 R_{max} surrounded by a rigid outer portion constrained not to move such that the total plate radius R_p =82.5 R_{max}. The flexible plate section is modeled with 20 axisymmetric "brick" elements (4 nodes each) for a total of 42 nodes. An additional 20 rigid fixed elements are employed in the outer rigid portion of the wall. The bubble is modeled with 24 axisymmetric panels. The plate material is taken as linear elastic with Young's modulus, $E = 3 \times 10^7 psi$, Poisson's ratio, $\nu = 0.3$, and a density such that the plate mass per unit surface area is 97 lbm/ft^2.

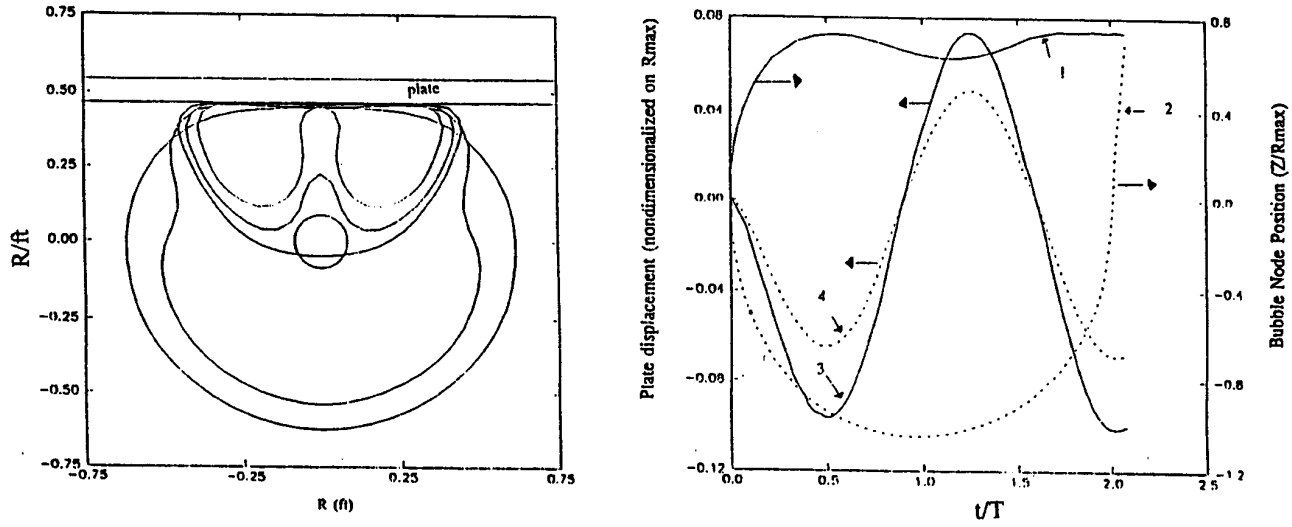

1: Bubble Node Nearest Plate. 2: Bubble Node Forming Jet. 3: Plate Center.
4: Plate Node at R=0.5R_f.

Figure 3: Deforming Plate. a) Bubble Growth and Collapse Contours. b) Plate Displacements and Bubble Node Positions.

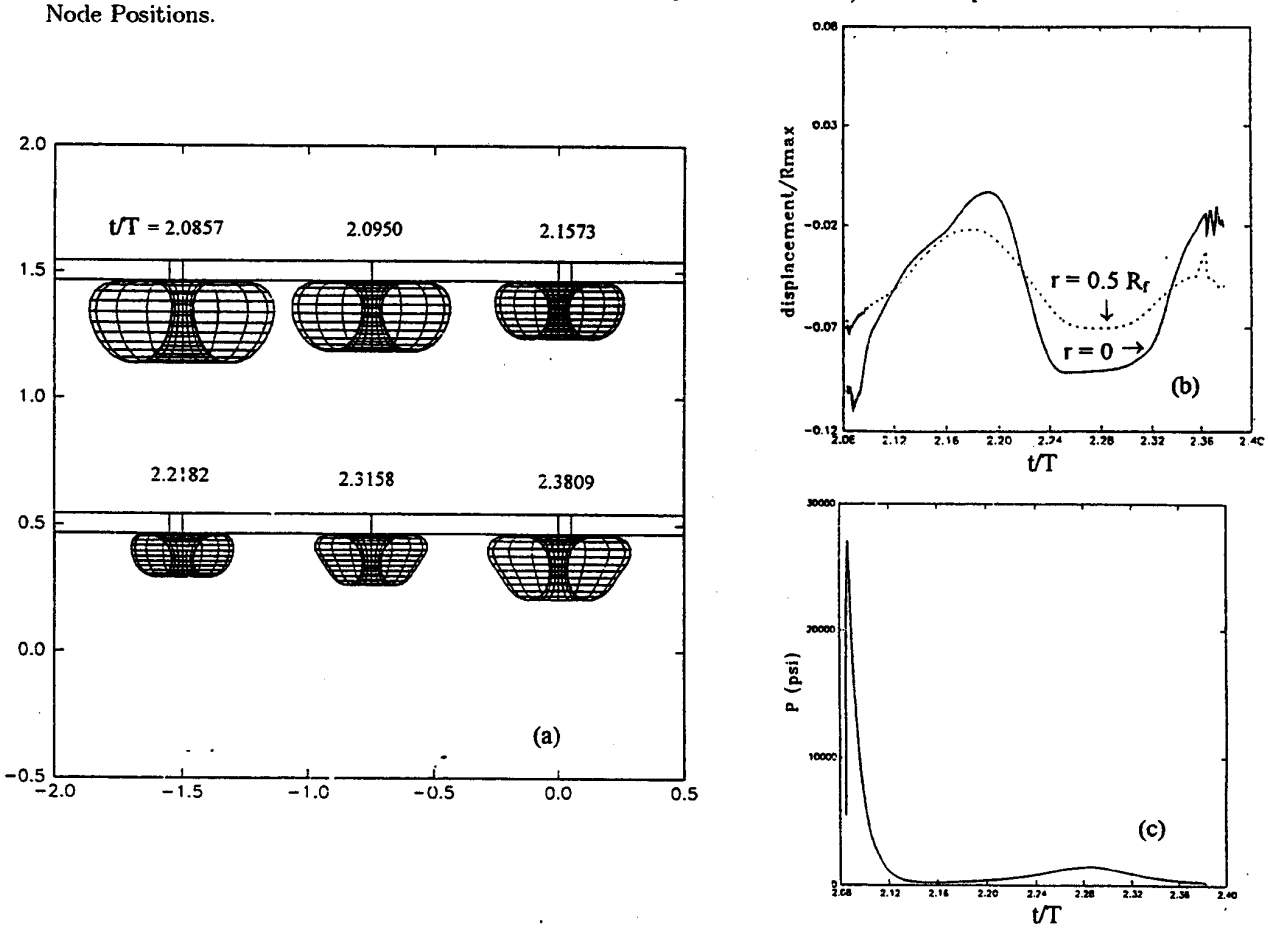

Figure 4: Post Touchdown Calculations for Deforming Plate. a) Bubble Shapes. b) Structural Displacements. c) Pressure at Plate Center Due to Jet Impact and Bubble Recompression.

Figure 3a presents a sequence of calculated bubble growth and collapse contours up to touchdown showing formation of the reentering jet. Figure 3b presents position histories of the bubble poles together with displacement histories of the plate center ($r = 0$) and a point located midway between the center and the flexible section outer edge ($r = R_f/2$). In this figure, a negative displacement represents an upward displacement. Thus the plate is initially deformed upward (away from the growing bubble), then moves toward the bubble when the bubble is near its maximum size, and is again deformed away from the bubble during bubble collapse, achieving maximum displacement near touchdown.

In Figure 4, these calculations were continued past touchdown and breakthrough with the techniques presented in [13]. During this post touchdown phase, the bubble achieves minimum volume and rebounds as shown in the contours of Figure 4a. Figure 4b presents post touchdown displacement histories of the same two points as in Figure 3b (Note that the time axis in Figure 4a has been expanded for clarity.) The displacement is seen to be driven by the bubble dynamics. Figure 4c presents the calculated post touchdown pressure history at the center of the plate. This exhibits the expected large pressure at touchdown and a second much smaller and broader pressure peak corresponding to minimum bubble volume.

Spherical Structures

This section presents results of example calculations performed utilizing the more powerful coupled **2DynaFS** - NIKE2D code. We first consider a bubble of initial radius $R_o = 0.177\ m$, and initial pressure $P_{go} = 6.83\ MPa$ growing and collapsing in a gravity field at a depth of 189 R_{max} above a spherical structure of radius 4 R_{max}. This is not representative of an explosive bubble, but is used for illustration of the spherical effects. The sphere is hollow with a thickness of 0.075 R_{max}. The gas constant used is $k = 1.25$. This results in a value of $T = 0.0146\ s$. The material model is *linear elastic* with Young's Modulus $E = 10,300 P_o$, Poisson's ratio $\nu = 0.3$, with a total mass $M = 225$ times the mass of water displaced by the bubble at its maximum size. The interior of the sphere is pressurized to P_0 to ensure initial equilibrium.

The bubble was discretized into 30 axisymmetric panels, and the spherical structure was discretized using four-noded axisymmetric continuum elements. In the results presented here, 60 elements were employed in the circumferential direction and 1 element in the thickness direction. Calculations performed with 2 elements in the thickness direction (120 total elements) showed no difference in the results with those with 1 element in the thickness direction. In performing the calculations for this set of parameters, it was found that the coupled calculation exhibits oscillations that were removed through the use of Rayleigh damping for the structure as described in [13,14].

The effects of structure motion and flexibility are presented in Figures 5-7. Calculated pressure histories at the structure node nearest the bubble are presented in Figure 5 for three structural conditions: fixed (rigid immoveable), rigidly moveable, and flexible. Calculations for three flexible structural damping conditions [13, 14] labeled 1,2,3 show little variation. The rigidly moving structure is seen to result in a slight reduction in the pressure generated, while structural flexibility is seen to result in a *reduction of the peak pressure by about 25%* relative to the fixed or rigidly moving structure cases. The bubble period is shortened by both rigid body motion and by structural flexibility as compared to the fixed case.

Figure 6 presents the bubble shapes at different times which exhibit a dramatic difference at the end of a bubble cycle of oscillation. In the rigid fixed body case the bubble collapses without significant jet formation, then forms a very thin jet during rebound. Best and Kucera found similar results near solid walls [15]. Lauterborn [16] has observed jet formation during rebound using laser generated bubbles. Subsequent bubble growth is such that the bubble practically touches the structure by the time the very thin jet impacts it. For the rigidly moving structure, a constriction develops on the top of the bubble prior to development of the reentrant jet. The later collapse of this constriction may correspond to the "counter-jet" observed in the experiments of Lauterborn & Bolle [17]. In the flexible wall case a constriction also develops on the top of the bubble followed by the beginning of a reentrant jet. However, the jet disappears as the bubble continues to grow during rebound.

The influence of the bubble on the structure can be seen in Figure 7 which presents the deformed structure shapes at three instants: during the growth, near maximum bubble size, and near the end of the collapse. In this figure, *the deformations have been exaggerated by a factor of 25 for clarity.* The influence of the loading by the bubble is apparent. During the early growth and at the time of collapse, the portion of the structure nearest the bubble (top) is pushed away from the bubble. Between these times, this portion of the structure is drawn toward the bubble.

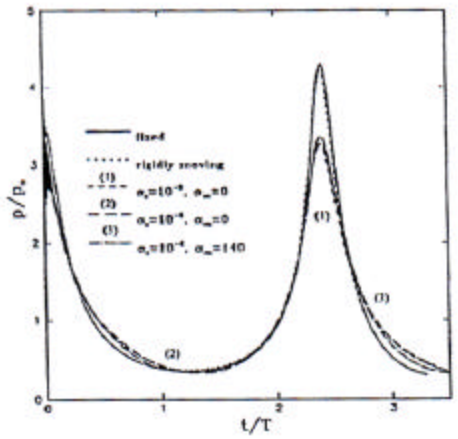

Figure 5: Bubble Growth and Collapse at a Standoff of 1.5 R_{max} above a Spherical Strucutre: Calculated Pressures Generated on Structure Node Nearest the Bubble.

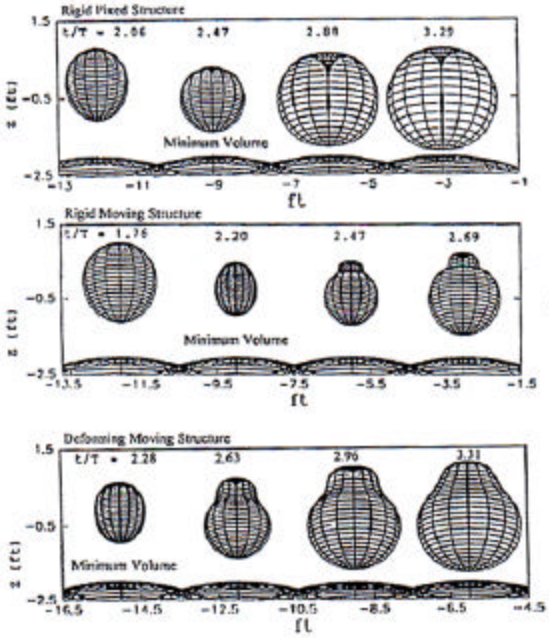

Figure 6: Comparison of Calculated Bubble Shapes During Collapse and Rebound for Case of Figure 5.

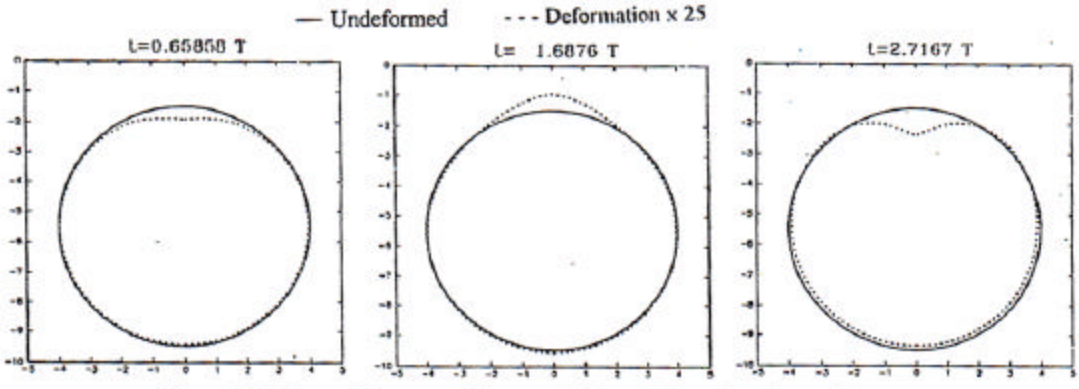

Figure 7: Deformed Structure Shapes at Selected Times for Case of Figures 5,6.

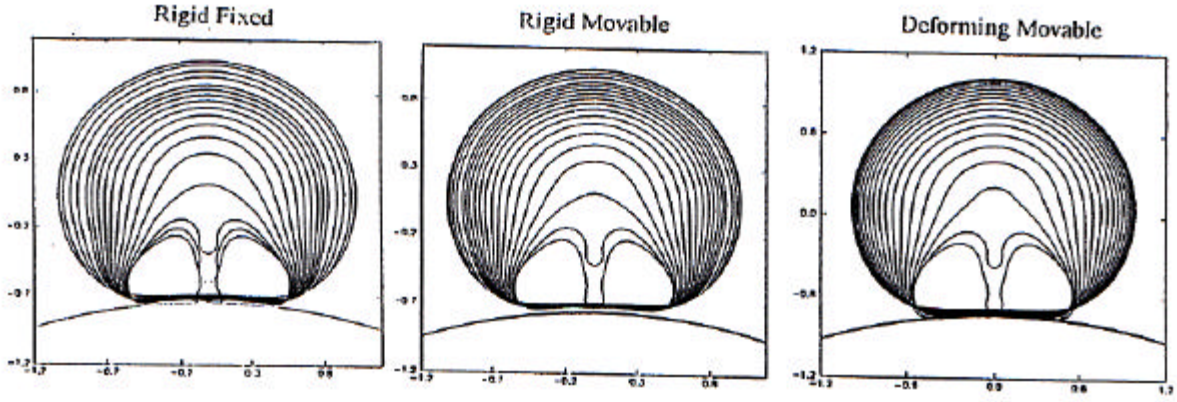

Figure 8: Calculated Bubble Collapse Contours for 0.75 R_{max} Standoff.

Figures 8 illustrates the capabilities of calculation of small standoff cases and presents the bubble shape contours from coupled calculations for the same conditions as above but with a standoff of 0.75 R_{max}. Little difference was observed between the fixed and the rigidly moving cases. However, the deformable case again showed a small shortening of the period [13].

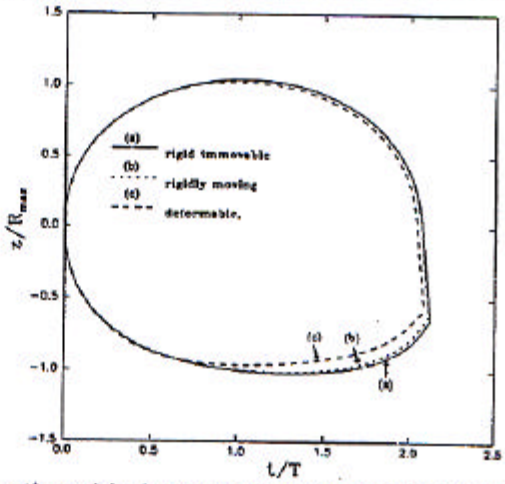

Figure 9: Calculated Position Histories of Top and Bottom Bubble Nodes for Bubble Generated by 0.5 lb of TNT at 1.5 R_{max} above a Spherical Structure.

Results of a simulation of a stronger bubble interacting with the same structure are presented in Figure 9. This case is that of an explosion bubble generated by 0.5 lb of TNT. Here the conditions, including R_{max}, are the same as for the example of figures 5 - 7 except that $R_o = 0.15 R_{max}$, $P_{go} = 106\ P_o$, and gravity effects are neglected. A strong reentry is seen for all three structural conditions: flexible, rigidly moving and rigid immovable. The bubble dynamics are quantitatively affected by the structural response as can be seen in Figure 9 which compares the position histories of the bubble nodes nearest and farthest from the structure. As before, rigid body motion is seen to shorten the bubble period while structural flexibility shortens the period even more relative to the rigid immovable case.

ANALYSIS OF A 3D CYLINDRICAL STRUCTURES

To account for the effects of bodily motion in response to the hydrodynamic forces generated by the bubble dynamics, a fully coupled general approach that allows for six degrees of freedom - translation and rotation about the x, y, and z directions - has been incorporated into **3DynaFS**. Details of this implementation can be found in [13].

Results of calculations are presented for the case of a bubble generated under the center of a submerged cylindrical body with its axis located along the x axis at a distance of 1.2 times the maximum bubble radius. In these calculations, one plane of symmetry was employed with a discretization consisting of 85 nodes and 144 triangular panels for the half bubble and 85 nodes and 156 triangular panels for the half body. The body was set to be *neutrally buoyant*.

Figure 10 shows the bubble contours and body cross sections at the $y = 0$ plane during bubble collapse. The contours appear qualitatively similar for the two cases. However, jet touchdown is seen to occur further

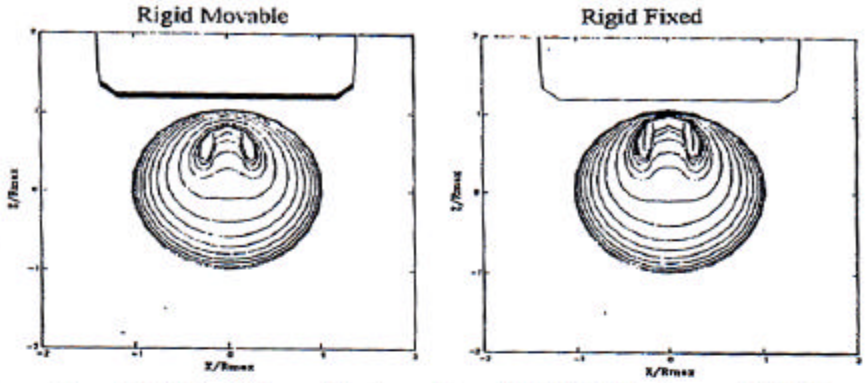

Figure 10: Comparison of Bubble Collapse Contours Beneath Rigidly Moving and Rigid Immoveable Bodies.

from the moveable body than from the immoveable body. Figure 11a presents the vertical (z) displacement and velocity histories of the moveable body. The body is seen to have an initial motion upward (away from the bubble), followed by a period of motion downward (toward the bubble). Finally the body experiences an upward acceleration (away from the bubble) during the end of the bubble collapse as can be seen by the change in its velocity. Due to inertia, the body has not yet begun to move away from the bubble at the time of touchdown although its advance downward has nearly ceased. The effect of the body motion on the bubble dynamics can be seen in Figure 11b which presents the position histories of the bubble north and south poles. The bubble collapse time when the body is allowed to move is decreased by a small amount relative to the base case. In addition, as also seen in Figure 10, the point of jet touchdown is found to move downward relative to the immoveable body case.

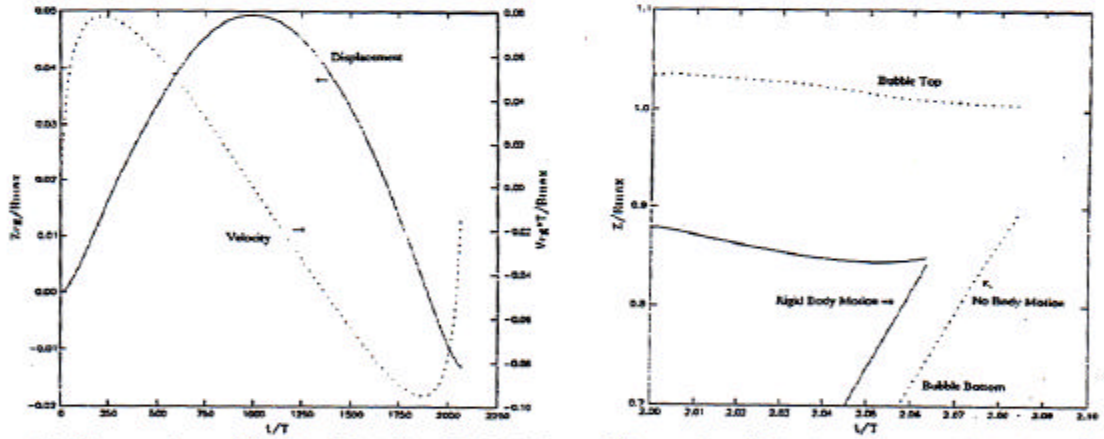

Figure 11: Comparison of Selected Details of Calculation of Figure 10. a) Displacement and Velocity of Body. b) Position Histories of Top and Bottom Bubble Nodes.

SUMMARY AND CONCLUSIONS

Results were presented from Boundary Element Method free surface hydrodynamics codes (**2DynaFS, 3DynaFS**) that were coupled to Finite Element Method structural dynamics codes (NIKE2D, NIKE3D) to study the effects of a deformable and movable interacting nearby structure on bubble dynamics. The results indicate potential for significant modification to the bubble behavior and its influence on the structure due to motion and deformation of the structure. In particular, bubble period modification accompanied by a modification of the reentrant jet formation and of the pressures generated along the solid body can be obtained. Bubble periods are seen to be shortened by interaction with a deformable structure while a smaller amount of shortening of bubble period is predicted for interaction with a rigid but movable structure. *The presence of a deformable structure is predicted to decrease the pressure along the structure* during bubble collapse compared to that on a rigid immovable structure. These results indicate that structural characteristics and the resulting structural response can affect loading caused by explosion bubbles. Simulation and prediction of these effects thus requires fully coupled fluid-structure modeling.

REFERENCES

1. Blake, J. R., Taib, B.B. and Doherty, G., "Transient Cavities Near Boundaries. Part I. Rigid Boundary," *Journal of Fluid Mechanics,* 1986, Vol. 170, pp. 479-497.
2. Blake, J. R, and Gibson, D. C., "Cavitation Bubbles Near Boundaries, " *Ann. Rev. Fl. Mech.,* 1987, Vol. 19, pp. 99-123.
3. Guerri, L., Lucca, G., and Prosperetti, A., "A Numerical Method for the Dynamics of Non-Spherical Cavitation Bubbles," *Proc. 2nd Int. Coll. on Drops and Bubbles,* JPL Publication 82-7, Monterey CA, November, 1981.
4. Wilkerson, S., "Boundary Integral Technique for Explosion Bubble Collapse Analysis," *ASME Energy Sources Technology Conference and Exhibition,* Houston TX., Jan.1989.
5. Chahine, G. L. and Perdue, T. O., "Simulation of the three-dimensional behavior of an unsteady large bubble near a structure," In *Drops and Bubbles,* 1989, (ed. T. G. Wang), *A.I.P. Conference Proceedings* **197**, 169-187.
6. Chahine, G. L., Perdue, T. O. & Tucker, C. B. 1989. "Interaction between an underwater explosion bubble and a solid submerged body, " DYNAFLOW, INC. Technical Report 89001-1.
7. Chahine, G. L., "Dynamics of the interaction of non-spherical cavities," in *Mathematical Approaches in Hydrodynamics,* 1991, (ed. T. Miloh), Philadelphia: SIAM, 51-67.
8. Maker, B. N., Ferenz, R. M. and Hallquist, J. O. November, 1990. "NIKE3D: a Nonlinear, Implicit Three-Dimensional Finite Element Code for Solid and Structural Mechanics, User's Manual," Lawrence Livermore National Lab Report UCRL-MA-105268.
9. Englemann, B., and Hallquist, J. O. April, 1991. "NIKE2D: a Nonlinear, Implicit, Two-Dimensional Finite Element Code for Solid Mechanics, User's Manual," Lawrence Livermore National Lab Report UCRL-MA-105413.
10. Chahine, G. L., Kalumuck, K. M. & Duraiswami, R., "Coupling of a fluids BEM code with a structural FEM code for fluid-structure interaction simulation. In *Boundary Elements XV, Proceedings of the 15th Boundary Element International Conference* (eds. C. A. Brebbia & J. J. Rencis),Worcester, MA. London: Elsevier, 1993, 581-596.
11. Chahine, G. L. & Duraiswami, R. 1993. "Boundary Element Method for Calculating 2-D and 3-D Underwater Explosion Bubble Behavior in Free Water and Near Structures," NSWC Weapons Research & Technology Department Report NSWC/TR-93/44 (limited distribution).
12. Whang, B., "Class Notes: Finite Element Methods in Engineering Mechanics," *Department of Civil, Mechanical and Environmental Engineering, George Washington University,* 1989.
13. Chahine, G. L., Duraiswami, R. & Kalumuck, K. M. 1995. "Boundary Element Method for Calculating 2-D and 3-D Underwater Explosion Bubble Loading on Nearby Structures Including Fluid-Structure Interaction Effects," NSWC Weapons Research & Technology Department Report NSWC/TR-93/46 (limited distribution).
14. Kalumuck, K.M., Duraiswami, R., and Chahine, G.L., "Bubble Dynamics Fluid-Structure Interaction Simulation by Coupling Fluid BEM and Structural FEM Codes," to appear, *J. Fluids and Structures.*
15. Best, J. P., and Kucera, A., "A Numerical Investigation of Non-spherical Rebounding Bubbles", *J. Fluid Mech.*, 1992, **245**, pp. 137-154.
16. Lauterborn, W., "Cavitation Bubble Dynamics - New Tools for an Intricate Problem." In *Mechanics and Physics of Bubbles in Liquids, IUTAM Symposium Proceedings,* June 1981, ed.: L. Van Wijngaarden.
17. Lauterborn, W. and Bolle, H., "Experimental Investigations of Cavitation Bubble Collapse in the Neighborhood of a Solid Boundary." *J. Fluid Mech.*, **1975, 72**, pp. 391-399.
18. Thrun. R., Goertner, J. F., and Harris, G. S., "Underwater Explosion Bubble Collapse Against a Flat Plate. 1992 Seneca Lake Test Series Data Report," NSWC Weapons Research & Technology Department Report NSWCDD/TR-92/482 (limited distribution).